CONCEPTS & SYNTHESIS
EMPHASIZING NEW IDEAS TO STIMULATE RESEARCH IN ECOLOGY

Ecology, 80(5), 1999, pp. 1475–1494

SEED DISPERSAL NEAR AND FAR: PATTERNS ACROSS TEMPERATE AND TROPICAL FORESTS

JAMES S. CLARK,[1] MILES SILMAN,[2] RUTH KERN,[3] ERIC MACKLIN,[4] AND JANNEKE HILLERISLAMBERS[1]

[1]*Department of Botany, Duke University, Durham, North Carolina 27708 USA*
[2]*Smithsonian Tropical Research Institute, Unit 0948, APO AA 34002-0948 USA*
[3]*Harvard Forest, Harvard University, P.O. Box 68, Petersham, Massachusetts 01366 USA*
[4]*Department of Organismic and Evolutionary Biology, Harvard University, 16 Divinity Avenue, Box 114, Cambridge, Massachusetts 02138 USA*

Abstract. Dispersal affects community dynamics and vegetation response to global change. Understanding these effects requires descriptions of dispersal at local and regional scales and statistical models that permit estimation. Classical models of dispersal describe local or long-distance dispersal, but not both. The lack of statistical methods means that models have rarely been fitted to seed dispersal in closed forests. We present a mixture model of dispersal that assumes a range of disperal patterns, both local and long distance. The bivariate Student's *t* or ''2Dt'' follows from an assumption that the distance parameter in a Gaussian model varies randomly, thus having a density of its own. We use an inverse approach to ''compete'' our mixture model against classical alternatives, using seed rain databases from temperate broadleaf, temperate mixed-conifer, and tropical floodplain forests. For most species, the 2Dt model fits dispersal data better than do classical models. The superior fit results from the potential for a convex shape near the source tree and a ''fat tail.'' Our parameter estimates have implications for community dynamics at local scales, for vegetation responses to global change at regional scales, and for differences in seed dispersal among biomes. The 2Dt model predicts that less seed travels beyond the immediate crown influence (<5 m) than is predicted under a Gaussian model, but that more seed travels longer distances (>30 m). Although Gaussian and exponential models predict slow population spread in the face of environmental change, our dispersal estimates suggest rapid spread. The preponderance of animal-dispersed and rare seed types in tropical forests results in noisier patterns of dispersal than occur in temperate hardwood and conifer stands.

Key words: Bayesian analysis; dispersal kernel; exponential model; forest dynamics; gamma; Gaussian model; migration; seed dispersal; seed shadow; Student's t.

INTRODUCTION

An understanding of dispersal is needed to assess recruitment limitation in plant communities and to predict population responses to global change (Schupp 1990, Ribbens et al. 1994, Pitelka et al. 1997, Clark et al. 1998*a*). Dispersal is summarized by a ''seed shadow,'' describing the density of juveniles with distance from the parent. A seed shadow model consists of two elements: (1) an estimate of fecundity, or the rate of seed production, and (2) a dispersal ''kernel,'' or probability density, describing the scatter of that seed about the parent. The seed shadow is the product of these two elements:

$$\text{seed shadow} = \text{fecundity} \times \text{dispersal kernel}$$

$$\left(\frac{\text{no. seeds}}{\text{m}^2\ \text{yr}}\right) = \left(\frac{\text{no. seeds}}{\text{yr}}\right) \times \left(\frac{1}{\text{m}^2}\right). \quad (1)$$

Seed shadows describe movement at several spatial scales. At fine scales, the fraction of seed that remains near the parent vs. that dispersed broadly affects aggregation and, thus, competition (Janzen 1970, Levin 1976, Geritz et al. 1984, Levin et al. 1984, Shmida and Ellner 1984, Augspurger and Franson 1988, Augspurger and Kitajima 1992, Venable and Brown 1993, Hurtt and Pacala 1996). At coarse scales, the seed shadow determines whether colonization of new habitats occurs

Manuscript received 2 January 1998; revised 18 August 1998; accepted 16 September 1998.

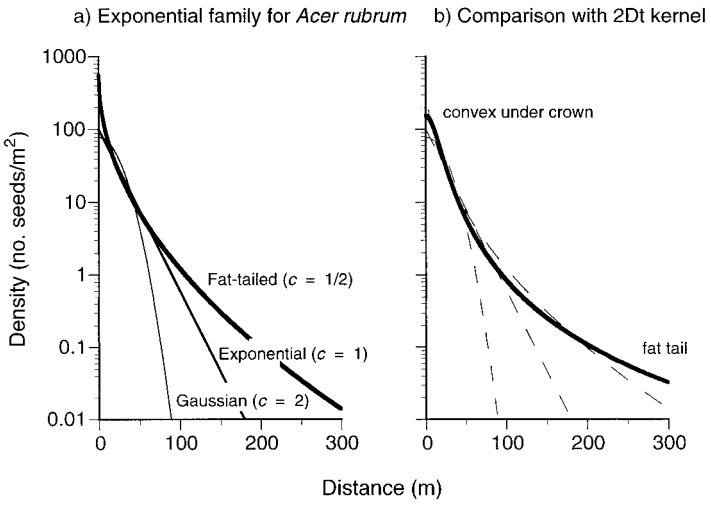

FIG. 1. Comparison of the shapes of kernel tails fitted to *Acer rubrum* seed rain. (a) Different models in an exponential family (Eq. 3) predict convexity at the source ($c > 1$) or a fat tail ($c < 1$), but not both. Exponential and fat-tailed kernels are more leptokurtic (more peaked and fat tailed) than is the Gaussian. (b) The 2Dt model (Eq. 7) predicts convexity at the source and a fat tail. Note the log scale of the *y*-axes.

mostly from patch edges, where seed rain from nearby adults is dense (Bjorkbom 1971, Hughes and Fahey 1988, Greene and Johnson 1989), or from seed traveling long distances (Davis 1981, Ritchie and MacDonald 1986, Fastie 1995). Plant migrations during climate change may be controlled by the ''tail'' of the kernel, with accelerating spread well in advance of the population frontier (Kot et al. 1996, Clark 1998). Taken together, these observations point to the need for an understanding of dispersal both near parent crowns and over long distances.

Two challenges stand in the way of predicting dispersal within natural communities. First is the need for kernel models that accurately describe dispersal across a range of spatial scales. The shapes of seed shadows assumed by dispersal biologists, modelers, and theorists reflect focus on a particular scale. Models applied at a fine scale usually assume a kernel that is convex near the source and platykurtic (e.g., the Gaussian kernel in Fig. 1a), because this shape describes the influence of the nearby (and sometimes overhanging) canopy (Green 1983, Geritz et al. 1984, Ribbens et al. 1994, Clark et al. 1998*b*). Seed density declines with distance from the parent tree, slowly at first, and then more rapidly beyond the crown edge. This ''local'' convexity requires a kernel $f(r)$ having a negative second derivative at the source, $d^2f(r)/dr^2|_{r=0} < 0$, where r is distance (Fig. 1a). Such dispersal kernels have been used to estimate probabilities of finding safe sites (Janzen 1970, Green 1983, Geritz et al. 1984), competition within tree communities (Ribbens et al. 1994), and recruitment limitation (Clark et al. 1998*b*). The restricted dispersal described by such kernels predicts species compositions that can contrast with those from models that assume global dispersal (Leishman et al. 1992, Hurtt and Pacala 1993, Ribbens et al. 1994, Clark and Ji 1995).

Ecologists concerned with processes that operate at broad spatial scales, such as reforestation of habitat fragments and population spread, commonly employ models that are concave near the source and leptokurtic (''fat-tailed'' in Fig. 1a). Exponential densities and power functions (Portnoy and Willson 1993, Willson 1993) are examples of models chosen principally for the shape of the ''tail'' of the seed shadow, i.e., on seed dispersed beyond the direct crown influence. Relatively small differences in the shapes of tails can have large effects on rates of population spread (Clark 1998). Platykurtic kernels estimated by dispersal biologists and community ecologists are of little use at coarse scales, whereas the leptokurtic models that appear more reasonable at coarse scales are likewise poorly suited for application at fine scales.

A second challenge has been the development of statistical methods for estimation and model testing. Past efforts to describe the scatter of seed about parent plants have enjoyed limited success. Observations from isolated trees in open or edge situations (Bjorkbom 1971, Smith 1975, Carkin et al. 1978, Gladstone 1979, Holthuijzen and Sharik 1985, Lamont 1985, Johnson 1988, Greene and Johnson 1989, Guevara and Laborde 1993) are hard to generalize to closed forests, because exposed crowns have higher seed production and are subject to different dispersal conditions than are their counterparts in closed stands (Ruth and Berntsen 1955, Fowells and Schubert 1956, Barrett 1966, Mair 1973). Seed shadows are a black box in models of stand dynamics, because there are no obvious ways to measure seed transport in closed canopies where seed shadows of individual trees overlap (Houle 1992, Martinez-Ramos and Soto-Castor 1993). Empirical approaches are summarized by a collection of functions (reviewed by Willson 1993) that are restricted in application to particular spatial scales and that yield inconsistent fits to data (Portnoy and Willson 1993). Although migration in response to global change has been critical to species

persistence, both past and present, seed dispersal has yet to be incorporated in Dynamic Global Vegetation Models (DGVMs), because existing empirical models are not relevant at coarse scales (Pitelka et al. 1997, Clark et al. 1998*a*).

Mechanistic approaches represent an alternative approach. Forces that act on an ensemble of seeds, including settling, diffusion, and advection (wind), are the components of Gaussian plume models. Applications to forest community dynamics are limited thus far (we are aware of none), because solutions generally assume simplistic boundary conditions (e.g., a point source) and constant wind profile. The distributed source, represented by a tree crown or by a stand of trees contributing seed to an open field (Okubo and Levin 1989), is responsible for the convex kernel shape close to that source. The ''skip distance'' predicted by a Gaussian plume model with an elevated point source and constant wind profile is not expected in real stands where winds vary and crowns are broad. Relaxing the assumption of a constant wind profile requires many parameters that are difficult to obtain and are dependent on specific conditions (Sharpe and Fields 1982, Andersen 1991).

Inverse modeling represents a powerful methodology for estimating fecundity and dispersal (Ribbens et al. 1994, Clark et al. 1998*a*, *b*). The approach uses the spatial pattern of seed recovered from seed traps and adult trees to statistically estimate the seed shadow. Although the transport of individual seeds is not observed, the model of seed arrival in traps can be inverted to provide parameter estimates, to estimate goodness-of-fit, and to propagate error. The methodology itself is quite general, accommodating a range of assumptions regarding kernel shape and error distribution. Alternative views of dispersal are represented by competing functional forms that can be compared based on field data.

Here, we integrate notions of dispersal that cut across spatial scales, and we determine the extent to which a classical vs. a new model derived from this integrated view explains dispersal in three biomes. The novel assumption of our model is that of a seed shadow constituting a continuous range of dispersal processes, including ones responsible for local (e.g., settling under conditions of light winds) to long-distance (e.g., movement by strong winds and transport by vertebrates) dispersal. This assumption is incorporated by modifying a standard dispersal model to include a density of dispersal parameters, with the resultant, new seed shadow being a ''continuous mixture.'' The resultant mixture model has desirable features at both local (i.e., convexity near the source) and long (i.e., high kurtosis, or a fat tail) distances. We then apply an inverse approach to parameterize the model, and we ''compete'' this model against the classical alternatives using data as arbitrator. Our tests are based on data from southern Appalachian, Sierra Nevada mixed-conifer, and Peruvian tropical floodplain forests. Comparisons demonstrate commonalities and differences across these contrasting biomes.

A Field Guide to Seed Shadows

A brief background summarizes differences among the dispersal kernels used to model dispersal, development of our new kernel, and inferences that can be drawn from our competitions among kernels using an inverse approach. We begin by describing a kernel in two dimensions, because this is a source of confusion in the literature.

A dispersal kernel in two dimensions

A tree's ''seed shadow,'' the flux of seeds at distance r (in meters), is the product of seed production rate Q (per year) and a density function, or kernel $f(r, \phi)$:

$$s(r, \phi) = Qf(r, \phi) \tag{2}$$

where ϕ is direction (e.g., radians), and $f(r, \phi)$ is seed density per square meter; Eq. 2 is a restatement of Eq. 1. We assume rotational symmetry, so direction ϕ is eventually suppressed; it is explicit initially to assure that we arrive at a proper normalization constant (a scalar guaranteeing that all seeds land somewhere). The probability that a seed originating at $r = 0$ falls on an area of ground surface (or in a seed trap) with diameter dr and subtending arc angle θ is the integral

$$\int_r^{r+dr} \oint_\theta f(r', \phi)\, d\phi\, dr' = \theta \int_r^{r+dr} r' f_\theta(r')\, dr' \approx \theta r f(r, \phi)\, dr. \tag{3}$$

Note that integration of $f(r, \phi)$ over arc angle θ yields $\theta r f_\theta(r)$. Integration over both θ and r yields a dimensionless fraction, which, upon multiplication by fecundity, gives the annual seed flux (i.e., number of seeds per year) to the area (θ, dr). This result is not the seed shadow of Eq. 2, which is a density and has units of number of seeds per square meter per year (Eq. 1), but, rather, the integration of it. The integration over 2π is $2\pi r f_{2\pi}(r)$, which is the marginal density for the random variable r. Moments represent a convenient summary of r and are solved in Appendix A. To simplify notation, we hereafter represent $f(r, \phi)$ as $f(r)$.

A family of dispersal kernels

Many functional forms can be, and have been, used to describe how offspring abundances vary with distance from the parent tree. We limit consideration here to proper density functions. We do not consider power functions, for example, because they contain a singularity (infinite density at zero); they cannot be parameterized to yield finite moments.

Many previous models and the new model developed here can be placed within the general context of one analyzed by Clark et al. (1998*b*):

$$f(r) = \frac{1}{N}\exp\left[-\left(\frac{r}{\alpha}\right)^c\right] \quad (4)$$

where α is a distance parameter (in meters), c is a dimensionless shape parameter, N is the normalization constant,

$$N = \int_0^\infty \oint_{2\pi} \exp\left[-\left(\frac{r}{\alpha}\right)^c\right] d\phi\, dr = \frac{2\pi\alpha^2\Gamma(2/c)}{c}$$

and

$$\Gamma(a) = \int_0^\infty z^{a-1}e^{-z}\, dz$$

is the gamma function. The kernel can be concave at the source and fat tailed ($c \leq 1$) or convex at the source and platykurtic ($c > 1$). The exponential ($c = 1$) is most common:

$$f(r) = \frac{1}{2\pi\alpha^2}\exp\left[-\frac{r}{\alpha}\right]. \quad (5a)$$

Alternative kernels in this family include the Gaussian ($c = 2$),

$$f(r) = \frac{1}{\pi\alpha^2}\exp\left[-\left(\frac{r}{\alpha}\right)^2\right]. \quad (5b)$$

Clark et al. (1998*a*) and various others; Ribbens et al. (1994) use $c = 3$, and Kot et al. (1996) and Clark (1998) use $c = 1/2$. Kurtosis, summarized from the second and fourth moments of the marginal density of r,

$$\frac{\mu_{R^4}}{\mu_{R^2}^2} = \frac{\Gamma(6/c)\Gamma(2/c)}{\Gamma^2(4/c)} \quad (6)$$

(see Appendix A), tends to infinity as c tends to zero and to zero as c becomes large. Thus, Eq. 4 accommodates the large kurtotsis that power functions attempt to capture, while still qualifying as a proper density function.

There are two limitations of dispersal kernels based on Eq. 4. First, although flexible (e.g., zero to infinite kurtosis), the seed shadow can be either convex at the source or leptokurtic, but not both (Fig. 1a). Second, statistical models used to fit kernels from seed or seedling data become unstable if estimation of α and c is attempted simultaneously. For five stands analyzed by Clark et al. (1998*b*), it was necessary to assume a value of c and then fit α. Ribbens et al. (1994) report similar difficulties. A more flexible kernel is obtained with a two-part model having ''local'' and ''long-distance'' components. The likelihood for this two-part model is ill-conditioned, however, prohibiting direct parameter estimation of the long-distance component (Clark 1998).

The Right Shape Near and Far: A Continuous Mixture

A kernel that accurately describes dispersal at both local and long-distance scales is obtained by characterizing the seed shadow as a composite process, summarized by a continuous range of dispersal parameters α. The Gaussian kernel (Eq. 5b) is a reasonable model for a restricted set of conditions. The model fits field data for most of the tree species that we tested, and species differences in dispersal parameters α matched closely the predictions based on fall velocities (Clark et al. 1998*b*). Nonetheless, the model is most sensitive to seeds dispersed over short distances, and it fails to describe sporadic seed dispersed over long distances: the tail of the kernel is essentially overlooked.

We modified the Gaussian kernel (Eq. 5b) by assuming that it varies continuously with prevailing conditions. For example, a small value of α might describe the kernel for seed released during times of light winds, whereas a large value might apply when winds are high, or for seeds dispersed by frugivorous birds, primates, or other vertebrates. Assuming then that α represents a random variable, we require a density of α values, call it $f(\alpha)$, to describe the probability of α values during seed release or transport. There are two restrictions on our choice for density $f(\alpha)$. First, it must be flexible. Second, it must have a form such that the product of $f(\alpha)$ and $f(r\,|\,\alpha)$ can be integrated to yield a new kernel $f(r)$ that incorporates variability in α. In other words, we must be able to solve for the marginal density $f(r)$ that results from the jointly distributed random variables r and α.

We searched for a density $f(\alpha)$ that is both flexible and permits a solution to (marginal density for) Eq. 5b. Such a solution is obtained by introducing a new variable A, that is defined in terms of α and scaling parameter u,

$$A \equiv \frac{u}{\alpha^2} \quad (7)$$

where A is gamma-distributed with shape parameter p:

$$f(A;\, p) = \frac{A^{p-1}e^{-A}}{\Gamma(p)}.$$

Writing Eq. 5b as a density $f(r\,|\,A)$ conditioned on the random variable A (which depends, in turn, on α), the new kernel becomes

$$f(r) = \int_0^\infty f(r\,|\,A)f(A)\, dA = \frac{p}{\pi u\left[1 + \dfrac{r^2}{u}\right]^{p+1}}. \quad (8)$$

A rescaling of parameters would show this to be a bivariate version of Student's t distribution. The density is two dimensional, because the normalization constant includes the arc-wise integration. Rotational symmetry suppresses arc angle, but the density is expressed per square meter rather than per meter. We therefore refer to this mixture as a ''two-dimensional t'' (2Dt) kernel. It tends to a Gaussian as p becomes large, and to a Cauchy as p tends to zero.

Advantages of our 2Dt mixture over variants on Eq. 3 are threefold. First, it has the right shape at local and long distances. Although convex at the source, it accommodates both fat and exponentially bounded tails. Moments $<2p$ are finite (Appendix A); thus, all moments are finite in the Gaussian limit ($p \to \infty$), and all are infinite in the Cauchy limit ($p \to 0$). Kurtosis (involving the fourth moment) is finite for $p > 2$.

A second advantage of the 2Dt distribution is the fact that the density of α is obtained as a by-product of fitting the kernel itself. Rather than simply obtaining best estimates of α and confidence intervals (e.g., Clark et al. 1998*b*), we obtain a full density of dispersal values with the variable change:

$$f(\alpha) = f(A)\left|\frac{dA}{d\alpha}\right| = \frac{2u^p}{\alpha^{2p+1}\Gamma(p)}\exp\left[-\frac{u}{\alpha^2}\right]. \quad (9)$$

This density can be viewed as a type of inverse χ^2. Moments of α can be expressed in terms of the moments of the kernel itself:

$$\mu_{\alpha^m} = \frac{2\mu_{R^m}}{m\Gamma(m/2)}.$$

These moments are finite so long as the corresponding moments of the kernel are finite. Thus, the mean of α is 1.12 times as large as the mean dispersal distance. The mode, which obtains at $d \ln f(\alpha)/d\alpha = 0$, is

$$\alpha_{\text{mode}} = \sqrt{\frac{2u}{2p+1}}.$$

A third advantage of this mixture is the fact that the density of α represents a conjugate prior for Bayesian estimation of the traditional exponential family (e.g., Gaussian and exponential). Although there is no such tractable Bayesian approach for the mixture likelihood that we will fit numerically, the conjugate pair provides a basis for rapid updating of exponential kernels from seed release data (Appendix B).

We will see that the 2Dt density is flexible and varies substantially among species. We interpret this density in terms of the mixture of processes that might contribute to dispersal.

Estimation: Inverting the Seed Shadow

The inverse problem presented by seed rain beneath closed canopies is summarized in Fig. 2. Multiple seed sources contribute to a given location. The seed rain from these multiple sources is a smoothed version of individual seed shadows, making it difficult to assign recovered seeds to specific sources. To avoid this problem, studies frequently focus on isolated trees in open fields or parking lots, at forest edges, or along hedgerows. We have noted that fecundities and transport at such locations are unrepresentative of closed canopies. It happens that the problem illustrated by Fig. 2 can be solved, in the sense that statistical estimates of the individual seed shadows can be obtained by inversion.

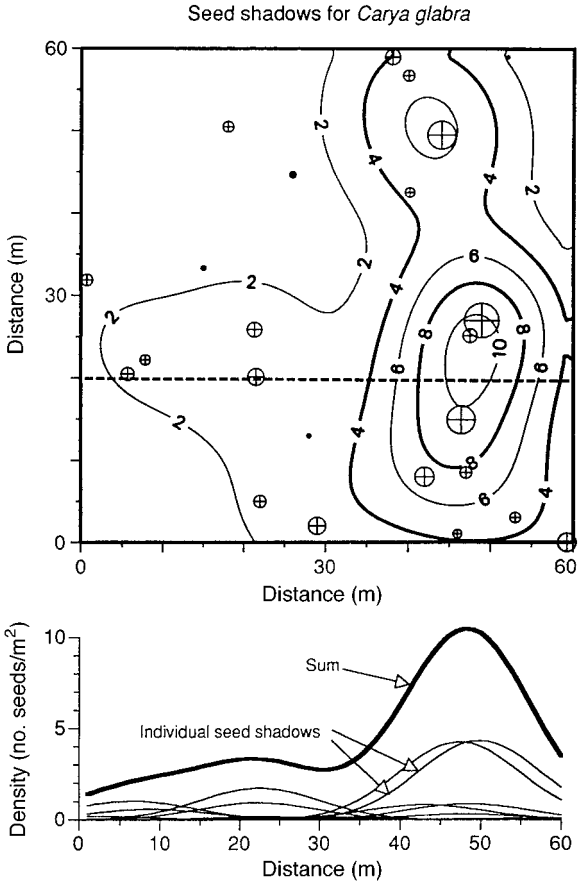

FIG. 2. The problem of estimating individual seed shadows when they overlap. The map shows individual trees (circles are scaled to relative diameter) and contours of seed density fitted by inverse modeling. The contours represent the sum of seed contributions from many nearby trees and thus are smoothed relative to individual seed shadows (lower panel, which shows a transect along the dashed line in the upper map). The individual seed shadows in the lower panel are estimated from total seed rain. The example here is from the temperate deciduous forest (Table 1).

The statistical model includes the two elements of the seed shadow (fecundity and a kernel from Eq. 1), together with a distribution of error.

Summed seed shadow model

Assume that overlapping seed shadows can be expressed as the summed contributions from each tree. Each seed shadow (Eq. 1) depends on distance and on tree size. The distance effect is simply the kernel $f(r)$ (Eq. 8). We assume that fecundity is proportional to basal area b (see also Ribbens et al. 1994):

$$Q(b) = \beta b, \quad (10)$$

where β is a parameter, because it represents the simplest assumption in light of few data. This assumption overestimates fecundity for old trees with senescing crowns, but more complex assumptions come at the cost of additional parameters. J. Clark (*unpublished*

TABLE 1. Forest stands used to model dispersal.

Forest type (location)	Annual precipitation (mm)	Elevation (m)	Stand number, type	Dominant species (based on basal area)
Temperate deciduous (35°03′ N, 83°27′ W)	1900	790	1, xeric ridge	*Quercus* spp., *Pinus rigida, Acer rubrum*
		800	2, cove hardwood	*Liriodendron tulipifera, Quercus* spp., *Acer rubrum*
		870	3, mixed oak	*Quercus* spp., *Acer rubrum, Carya glabra*
		1090	4, mixed oak	*Quercus* spp., *Acer rubrum, Nyssa sylvatica*
		1390	5, northern hardwood	*Betula* spp., *Quercus* spp., *Tilia americana*
Temperate mixed-conifer (36°34′ N, 118°46′ W)	1000	2200	1, Sierra Nevada mixed-conifer	*Abies concolor, Abies magnifica* var. *shastensis, Sequoiadendron giganteum*
		2200	2, sequoia–mixed-conifer	*Sequoiadendron giganteum, Abies concolor, Abies magnifica* var. *shastensis*
		1600	3, Sierra Nevada mixed-conifer	*Calocedrus decurrens, Abies concolor, Quercus kelloggii*
		1600	4, Sierra Nevada mixed-conifer	*Calocedrus decurrens, Quercus kelloggii, Pinus ponderosa*
Tropical floodplain (11°54′ S, 71°22′ W)	2000	350		*Otoba parvifolia, Quararibea witti*

manuscript) is examining nonlinear fecundity models for one of our data sets. In most cases, Eq. 10 fits the data better than do more complex assumptions.

The model of seed rain is the sum of individual seed shadows in Eq. 2. Using functional forms for Q (Eq. 10) and $f(r)$ (Eq. 8), we write the summed model as

$$\hat{s}(\mathbf{b}, \mathbf{r}_j; \varphi_z) = \sum_{i=1}^{m\text{trees}} \beta b_i f(r_{ij}; u, p) \qquad (11)$$

where $\hat{s}(\mathbf{b}, \mathbf{r}_j; \varphi_z)$ is the seed density predicted at seed trap j, based on an m-length vector of tree basal areas $\mathbf{b}$, an $m \times n$ matrix of distances $\mathbf{r}$, and a vector of z fitted parameters, which, for the 2Dt model in Eq. 8, is $\varphi_z = [\beta, u, p]$. We find parameter values that fit the ''sum'' in Fig. 2, which, by implication, allows us to draw the ''individual seed shadows'' that together define that sum.

Likelihood: data and distribution of error

Assuming a model, the likelihood of obtaining a data set is the joint likelihood (i.e., product) of observing each datum. Our data consist of mapped tree plots with seed traps in three forests (Table 1). Stand composition, dispersal biology, and data sets are described elsewhere (Clark et al. 1998*b*; M. Silman and J. Clark, *unpublished manuscript*; R. Kern et al., *unpublished manuscript*). In brief, mapped stands include the location (coordinates), diameter at breast height, and species of each tree. The finite areas of our maps (Table 2) can affect parameter estimates for the best dispersed species (*Betula*, *Liriodendron*) only on our smallest plots, those from the southern Appalachians (Clark et al. 1998*b*). Seeds were identified to the lowest possible taxonomic unit and were expressed as density per year. Each datum is the seed accumulation in one seed trap, averaged over the duration of the study (Table 2).

Seed traps do not receive precisely the number of seeds predicted by Eq. 11, but rather some stochastic realization of it. The error distribution describes the scatter of seed densities about the mean value predicted by the seed shadow. Clark et al. (1998*b*) used a negative binomial, because seed rain was found to be more clumped than a Poisson distribution. The negative binomial permits this clumping at the cost of an extra fitted parameter. Because our mixture kernel introduces a random variable (α) that tends to accommodate additional variability, our attempts to fit the 2Dt kernel with negative binomial error resulted in unstable parameter estimates. We therefore use the Poisson likelihood:

TABLE 2. Summary of data sets analyzed in this study.

Forest type	No. stands (q)	Area of each stand (ha)	No. seed traps per stand	Area per seed trap (m^2)	Duration (yr)
Temperate deciduous	5	0.36	20	0.18	5
Temperate mixed-conifer	4	1.0–2.5	25	0.25	3–4†
Tropic floodplain	1	2.25	40	0.50	2

† Durations of seed collections were four years in stand 1 and three years in all others.

$$L(\mathbf{S}\,|\,\varphi_z) = \prod_{j=1}^{n} \frac{\hat{s}(\mathbf{b}, \mathbf{r}_j; \varphi_z)^{s_j} \exp(-\hat{s}[\mathbf{b}, \mathbf{r}_j; \varphi_z])}{s_j!} \quad (12)$$

where **S** is an n-length vector of observed seed densities (seed trap counts), and s_j is the observed density of seed in trap j. Although we do not observe the travel from trees to seed traps, the likelihood (Eq. 12) provides a means for ''inverting'' the problem and, thus, estimating parameters.

Parameter estimation for the alternative dispersal models (Eqs. 5a, b, 8) follows Clark et al. (1998*b*). We outline the approach for the 2Dt kernel, because similar methodology applies to the exponential (5a) and Gaussian (5b) models. Maximum likelihood (ML) estimates for the parameter vector $\varphi = [u, \beta, p]$ maximize the likelihood of observing data set **S** (Eq. 12), given the model represented by Eq. 11. In numerically minimizing Eq. 12, we constrained our search for p estimates on the interval (1/2, 10), because a tendency for correlation between parameters p and u in bootstrapped estimates outside this range became severe. In most cases, fitted p values tended to low values (1/2), indicating a fat-tailed kernel. Less frequently, p tended to high values, or a Gaussian kernel. We determined 95% confidence intervals on parameters, and we propagated error through the seed shadow $s(r)$ and the density of α values, $f(\alpha)$. We bootstrapped 500 estimates on resamples (with replacement) from seed traps, and we constructed corresponding $s(r)$ and $f(\alpha)$ functions for each resample. Our method is Efron and Tibshirani's (1993) ''nonparametric'' bootstrap; we sample directly from the data rather than from a parametric distribution. Confidence intervals are 95% quantiles of each parameter and at 1-m intervals for $f(r)$ and $f(\alpha)$. Clark et al. (1998*b*) found that bias-corrected and accelerated confidence intervals (Efron and Tishirani 1993) did not differ substantially from simple bootstrapped quantiles, so we report quantiles here. Confidence intervals about the functions $s(r)$ and $f(\alpha)$ propagate parameter error and correlation through to the confidence in the seed shadow and in the density of dispersal variables.

We estimated parameters for one to several stands for data sets having more than one stand (temperate deciduous and temperate mixed-conifer). Some species were too rare to obtain fits in all stands. In a few cases, trees were so abundant that seed rain was too uniform across plots to permit parameter estimates. Thus, each fit is obtained on $q \leq 5$ (temperate deciduous) or $q \leq 4$ (temperate mixed-conifer) stands, with the likelihood

$$L(\mathbf{S}_q\,|\,\varphi) = \sum_{k=1}^{q\text{stands}} L(\mathbf{S}_k\,|\,\varphi). \quad (13)$$

$L(\mathbf{S}_k\,|\,\varphi)$ is the likelihood of the data observed in the kth stand (Eq. 12). The vector of fitted parameters φ depends on q and on one of several hypotheses that we tested from our data. We report a weighted r^2 as a goodness-of-fit index, where weights are variance estimates taken as the predicted mean for this Poisson model.

Which model is best?

Hypothesis tests were used to assess parameter consistency and to guide model selection. Data were used to arbitrate among three competing models (Gaussian, exponential, and 2Dt) on the basis of likelihoods. The Gaussian model (parameter vector $\varphi = [\beta, \alpha]$) is nested within the 2Dt model, being obtained in the limit as p becomes large. Although nested, the classical likelihood ratio test with 1 df is not quite correct. Because the Gaussian obtains at the boundary $p \to \infty$, the likelihood ratio is a mixture of χ^2 distributions having 0 and 1 df, each with probability 1/2, the former being a delta function centered on zero (Chernoff 1954). Probabilities for our comparisons of Gaussian vs. 2Dt use this mixed distribution.

The exponential model (parameter vector $\varphi = [\beta, \alpha]$) differs from the Gaussian only in the value of the exponent (c in Eq. 4), so the best fitting model is that having the lowest $-\ln L$. For comparing the ''generalized exponential'' and 2Dt models, we treated parameter c in Eq. 4 as a fitted parameter to give parameter vector $\varphi = [\beta, \alpha, c]$. These two models are not nested, but they contain the same number of parameters (3); the best fitting model is simply the one with the lowest $-\ln L$. Our parameter search for c was bounded on (1, 4), because parameter correlations became severe for $c < 1$, and likelihoods were insensitive to values of $c > 4$.

Hypothesis tests for goodness-of-fit

Hypothesis testing for the 2Dt kernel follows Clark et al. (1998*b*). Provided that parameters (and the seed shadows they represent) are consistent from stand to stand, the most general parameter estimates come when fitted simultaneously to all stands having sufficient trees and seeds of a species. Three parameters represent the fits obtained when all possible information is included:

$$\mathbf{p}_3 = [\beta, u, p]. \quad (14)$$

The null model is simply the Poisson, where each seed trap receives the mean density. The deviance

$$D_2 = -2 \ln\left[\frac{L(\mathbf{S}_q\,|\,\mathbf{p}_3)}{L(\mathbf{S}_q\,|\,\bar{s})}\right] \quad (15)$$

is distributed as χ^2 with 2 degrees of freedom, three parameters for the fitted model minus one (the mean) for the null Poisson.

Although Eq. 14 includes the maximum information on the seed shadow for a species, we tested whether dispersal differs among plots by comparing this ''global'' seed shadow with the likelihood of the data under the hypothesis of q different seed shadows (i.e., a seed shadow differs from plot to plot) with parameter vector

$$\mathbf{p}_{2q+1} = [\beta_1, \ldots, \beta_q, u_1, \ldots, u_q, p]. \quad (16)$$

The hypothesis of q different seed shadows is tested using the likelihood ratio test, where the deviance

$$D_{2(q-1)} = -2 \ln\left[\frac{L(\mathbf{S}_q|\mathbf{p}_{2q+1}}{L(\mathbf{S}_q|\mathbf{p}_3)}\right] \quad (17)$$

is asymptotically distributed as χ^2 with $2(q - 1)$ degrees of freedom (difference in the number of parameters for Eqs. 14 and 16). Clark et al. (1998*b*) present tests for fecundity differences among plots. For species having significant differences in seed shadows among stands (deviance 17), we fitted an additional model to determine whether dispersal was consistent among plots. The parameter vector for stand-specific fecundity fits is

$$\mathbf{p}_{q+2} = [\beta_1, \ldots, \beta_q, u, p]. \quad (18)$$

We tested for dispersal differences with the deviance

$$D_{q-1} = -2 \ln\left[\frac{L(\mathbf{S}_q|\mathbf{p}_{2q+1}}{L(\mathbf{S}_q|\mathbf{p}_{q+2})}\right] \quad (19)$$

for parameter vectors given by Eqs. 16 and 18 with $q - 1$ degrees of freedom. Dispersal distance is judged ''inconsistent'' among stands if plot-specific dispersal parameters (Eq. 16) substantially improve the fit over that obtained with a single, ''global'' dispersal parameter (Eq. 18). The null model for the likelihood fitted to Eq. 18 is

$$D_{q+2} = -2 \ln\left[\frac{L(\mathbf{S}_q|\mathbf{p}_{2(q+1)}}{L(\mathbf{S}_q|\bar{s}_q)}\right] \quad (20)$$

which has $q + 2$ degrees of freedom, $2(q + 1)$ parameters for the fitted model minus q means.

For some species having fecundity differences among stands, we still report the ''global'' seed shadow obtained for multiple stands. Large sample sizes could always produce significant differences among stands, but those differences should not obscure the search for a general model. Although we report results for both models, we focus on results of the global model.

Results

The 2Dt model provided the best fit for most species (Table 3). The cases in which the 2Dt did not outperform other models were mostly those for which confident fits could not be obtained for any of the three models. The Gaussian model provided the best fit mostly for animal-dispersed species (*Castanea dentata*, *Quercus* spp., *Quararibea witti*, *Sapium marmieri*, and *Spondias mombin*). There were three exceptions in which wind-dispersed species were best fit by the Gaussian model (*Tsuga canadensis*, *Abies magnifica* var. *shastensis*, and *Pinus ponderosa*), two of which (*T. canadensis* and *P. ponderosa*) did not significantly improve on the null Poisson model and had low weighted r^2 values (Table 4). The sole case in which a platykurtic model provided the best fit was for an animal-

Table 3. Goodness-of-fit for competing dispersal kernels. Likelihoods for best fitting models are in boldface. Probabilities for 2Dt (in parentheses) are for likelihood ratio tests against the Gaussian model.

Species	−ln *L* 2Dt	−ln *L* Gaussian	−ln *L* Exponential family†
a) Temperate deciduous, wind-dispersed			
Acer rubrum	1059 (<0.001)	1089	**1045**
Betula lenta	**8155** (<0.001)	8297	8196
Fraxinus americana	**108** (0.0039)	227	**108**
Liriodendron tulipifera	**2250** (<0.001)	4701	**2250**
Pinus rigida	**92.1** (0.001)	99.4	95.9
Tilia americana	**765** (<0.001)	890	824
Tsuga canadensis	99.6 (0.297)	**99.8**	99.6
b) Temperate deciduous, animal-dispersed			
Castanea dentata	15.9	**15.9**	17.8
Carya spp.	**196** (<0.001)	260	215
Cornus florida	**122** (<0.001)	180	138
Nyssa sylvatica	**493** (<0.001)	745	580
Quercus spp.	880	**880**	933
c) Temperate mixed-conifer			
Abies concolor	**983** (0.028)	985	997
Abies magnifica var. *shastensis*	557	**557**	571
Pinus lambertiana	**31.1** (0.044)	32.5	31.7
Pinus ponderosa	22.6	**22.6**	22.5
Sequoiadendron giganteum	**109** (<0.001)	139	119
d) Tropical floodplain			
Calycophyllum spruceanum	**281** (<0.001)	322	295
Hyeronima laxiflora	**111** (<0.001)	129	121
Iriartea deltoidea	91.8	91.8	**88.7**†
Quararibea witti	16.8 (0.12)	**17.5**	17.0
Sapium marmieri	80.8	**80.8**	80.8†
Spondias mombin	3.42	**3.42**	3.07
Virola sebifera	**18.0** (0.0089)	20.8	19.0
Number of wins‡	14	8	4§

† The ''exponential family'' has $c = 1$ in all cases except *Iriartea deltoidea* and *Sapium marmieri*, where $c > 4$ constituted the best fit.

‡ The total number of cases in which a model represented the best fit.

§ Three wins with $c = 1$ and one win with $c > 2$.

TABLE 4. Parameter estimates for 2Dt model. For cases in which a single fecundity parameter β did not provide a fit, the seed shadow was fitted with a separate β for each stand.

Species and stand numbers	Parameter ± SE: Fecundity β (no. seeds/cm² basal area)	Dispersal u (m²)	p (dimensionless)	α_{mode} (m)	Kurtosis	H_0: Poisson seed rain‡	H_0: dispersal consistent§	Weighted r^2
a) Temperate deciduous, wind-dispersed								
Acer rubrum (1, 2, 3, 4, 5)	84.1 ± 19.9	602 ± 400†	<0.5	24.5	∞	0	0	0.86
Betula lenta (1, 2, 3, 4)	1084 ± 318	777 ± 734†	<0.5	27.9	∞	0	0	0.95
Fraxinus americana 5	8.32 ± 4.51	217 ± 627†	<0.5	14.7	∞	0		0.37
Liriodendron tulipifera (1, 2, 3, 4)	73.0 ± 13.5	302 ± 165†	<0.5	17.4	∞	0	0	0.98
Pinus rigida 1	2.19 ± 5.94	18.6 ± 332	<0.5	4.31	∞	0		0.74
Tilia americana (2, 5)	17.3 ± 4.87	10.4 ± 102†	<0.5	3.22	∞	0	0	0.56
Tsuga canadensis (1, 2, 4)	27.8 ± 18.6	1839 ± 1980†	<0.5	42.9	∞	0.90	0	0.41
b) Temperate deciduous, animal-dispersed								
Castanea dentata								
1	5.63 ± 65.9	141 ± 55.2	>10	3.66	2	0	0	0.95
4	0.209 ± 22.42							
Carya glabra (1, 2, 3, 4, 5)	1.38 ± 0.231	8.82 ± 60.8	<0.5	2.97	∞	0	0	0.82
Cornus florida								
1	13.1 ± 6.36	4.48 ± 76.0	0.61 ± 0.224	2.00	∞	0	0	0.63
2	2.35 ± 3.11							
3	1.40 ± 21.8							
4	0.798 ± 2.29							
Nyssa sylvatica (1, 2, 3, 4)	9.82 ± 2.50	1.91 ± 148	<0.5	1.38	∞	0	0	0.92
Quercus								
1	2.24 ± 0.369	1893 ± 751	>10	13.4	2	0	0	0.63
2	1.30 ± 0.417							
3	0.526 ± 0.107							
5	6.08 ± 2.46							
c) Temperate mixed-conifer								
Abies concolor (1, 2, 3, 4)	3.20 ± 0.236	552 ± 335	6.57 ± 3.03	8.83	2.44	0	0	0.92
Abies magnifica var. *shastensis* (3, 4)	7.24 ± 0.704	7511 ± 2372†	>10	26.7	2	0	0	0.48
Pinus lambertiana (3, 4)	0.342 ± 0.110	175 ± 346	<0.5	13.2	∞	0.00016	0.017	0.84
Pinus ponderosa 2	0.145 ± 0.0544	2645 ± 3528	>10	15.9	2	0.11		0.22
Sequoiadendron giganteum (3, 4)	0.632 ± 0.0508	109 ± 16.1	<0.5	10.4	∞	0	0.035	0.98
d) Tropical floodplain								
Calycophyllum spruceanum	17.9 ± 79.5	195 ± 758	2.94 ± 3.31	7.52	∞	0		0.97
Hyeronima laxiflora	‖	17.4 ± 1401†	0.816 ± 2.80	2.24	∞	0		0.83
Iriartea deltoidea	1.42 ± 10.2	5378 ± 2662	>10	22.6	2	0		0.27
Quararibea witti	0.24 ± 0.185	7.82 ± 1100	<0.5	2.80	∞	0.0017		0.28
Sapium marmieri	2.17 ± 1.10	6104 ± 3373	>10	24.1	2	0		0.42
Spondias mombin	0.0438 ± 0.127	996 ± 246	>10	9.74	2	0.012		0.97
Virola sebifera	1.17 ± 21.0	163 ± 366	1.82 ± 4.01	8.38	∞	0		0.91

† Fits for which correlation between parameters β and u exceeds |0.5|.
‡ P values for the null hypothesis that dispersal is independent of trees, using deviances in Eqs. 15 or 20, depending on numbers of plots.
§ P values for the hypothesis that dispersal parameters u differ among plots, tested with the deviance given by Eq. 19.
‖ Model instability for the sparse data precluded estimation of a fecundity parameter for *Hyeronima laxiflora*.

dispersed species (*Iriartea deltoidea*, $c > 4$), and the fit was marginal (weighted $r^2 = 0.158$). The exponential model was the best fitting model in only one case (*Acer rubrum*), and it provided as good a fit as the 2Dt model for two other wind-dispersed species (*Fraxinus americana* and *Liriodendron tulipifera*).

Good fits for the 2Dt model result from its potential to admit large kurtosis. The few cases in which the Gaussian model provided the best fit were those for which the shape parameter p tended to high (>10) values (Table 4), simply indicating the Gaussian limit of the 2Dt model as p becomes large. The 2Dt model

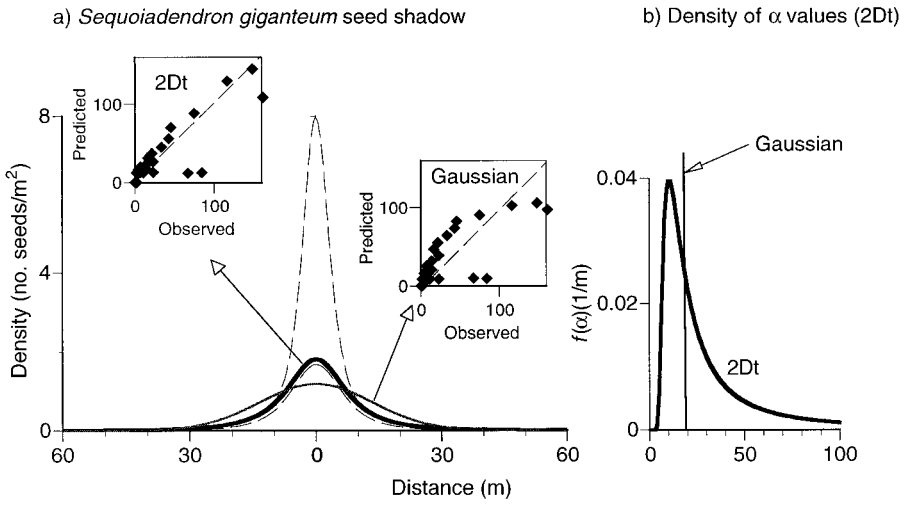

FIG. 3. Demonstration of how the 2Dt model better describes seed rain data than does the Gaussian model for most of the species that we analyzed. (a) The predicted seed shadows include the 2Dt model with dashed 95% confidence intervals and the more platykurtic Gaussian fit. Insets demonstrate the observed and predicted values with the dashed line of agreement. The likelihood ratio test for this comparison is included in Table 3. (b) The density of α values (dispersal parameters) for the seed shadow in (a) compared with the maximum likelihood (ML) estimate for the Gaussian model (arrow).

provided a better fit than the Gaussian in most cases, because the convexity near the source captures the high seed densities directly beneath canopies, whereas the fat tail describes more distant travel. *Sequoiadendron giganteum* is a typical example (Fig. 3a, b). Like the 2Dt, the Gaussian model is convex at the source, but it ''splits the difference'' between local and long-distance dispersal, causing it to underestimate the source and overestimate intermediate distances (Fig. 3a, insets). The *Sequoiadendron* kernel implies a broad range of α values (Fig. 3b).

Fecundity variability among stands for the 2Dt model was similar to that obtained by Clark et al. (1998*b*) for a Gaussian model, but dispersal variability among stands for the 2Dt was consistently high. Species having significant fecundity differences among stands (*Castanea*, *Cornus*, and *Quercus*) are dispersed by animals. Unlike the Gaussian model, which rarely obtained better fits for stand-specific α estimates (Clark et al. 1998*b*), only one species (*Sequoiadendron*) was best described by a stand-specific estimate of *u*.

The correlation among species in fecundity and dispersal for temperate species (Clark et al. 1998*b*) applies, to a lesser degree, across the three forest types examined here (Fig. 4). Animal-dispersed species (''temperate, animal'' and most ''tropical floodplain'' in Fig. 4) tended to have lower fecundity estimates and lower modal dispersal than did wind-dispersed deciduous species. Mixed conifers had lower fecundities than did their wind-dispersed, deciduous counterparts (Table 4). Although they generally had low fecundities, the restricted dispersal of animal-dispersed species meant that their seed densities near adult trees were as great as those of the more fecund, wind-dispersed species (Fig. 5).

Fig. 5 illustrates the fat tails that best describe seed shadows for most species. Although convex near the source, most kernels flatten with distance, approaching zero more slowly than exponential (Fig. 1). Kurtosis

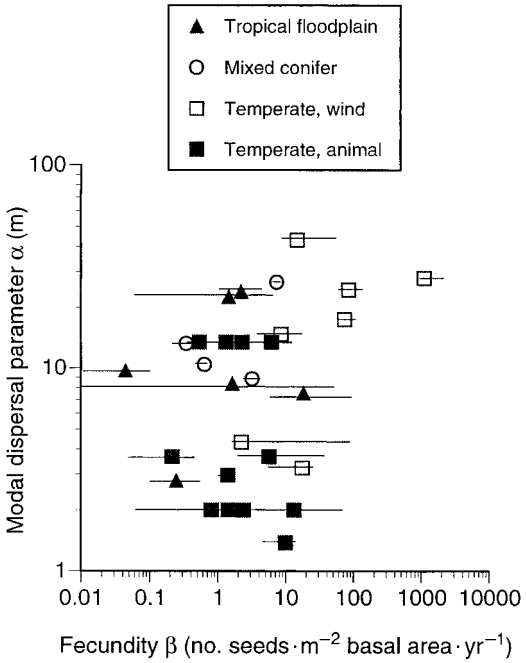

FIG. 4. Fecundity parameter estimates (with 95% confidence intervals) and modal dispersal parameters from the 2Dt model. Note the log scales.

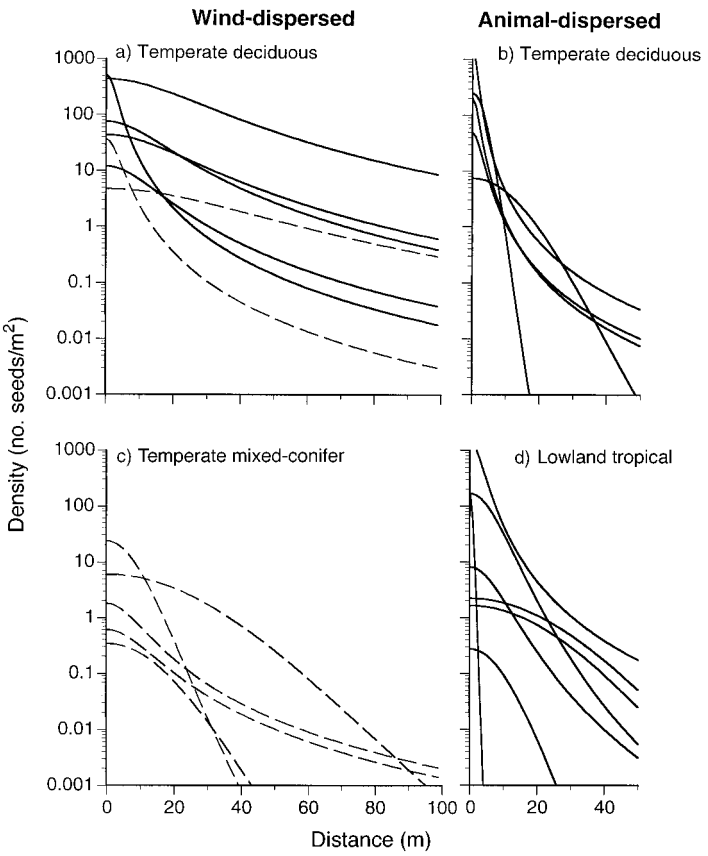

FIG. 5. Maximum-likelihood seed-shadow estimates. Confidence intervals are omitted for clarity. Dashed lines indicate conifers. Note the *y*-axis log scale.

estimates for these fitted seed shadows are not finite (Table 4). Densities of the dispersal parameter $f(\alpha)$ are likewise fat tailed (Fig. 6). Wind-dispersed types have broad densities of α ranging from 5 to 100 m, whereas animal-dispersed types have values concentrated at $<$10 m (Fig. 6, insets).

The flexibility of the 2Dt kernel, which allows for superior fits in Table 3, is cause for instability when data are sparse. Although *Hyeronima laxiflora* was best fitted by the 2Dt (Table 3), the model was unable to resolve parameter estimates. Large accumulation near a single adult tree appears as an outlier (insets in Fig. 7a). The ''inflexibility'' of the Gaussian model allowed us to obtain stable parameter estimates for these data (M. Silman and J. Clark, *unpublished manuscript*). The 2Dt, however, finds a continuous range of parameters to fit the scatter of data by trading off fecundity and dispersal parameters. Negative correlation between β and α is responsible for wide confidence intervals on the seed shadow (Fig. 7a) and for bimodal confidence intervals on $f(\alpha)$ (Fig. 7b).

The 2Dt is unstable at extreme values of *p*. Although stabilized by our truncated search interval of $1/2 \leq p \leq 10$, there was greater parameter correlation in this model (Table 4) than for the Gaussian (Clark et al. 1998*b*: Table 3). Parameter *p* is especially susceptible, because *p* can have a small effect on the likelihood, and it can be offset by trade-offs with *u*. This tendency is reduced by adequate distribution of data and by sufficiently long-term data sets to average over noise. Parameter correlation in the 2Dt model is greatest for wind-dispersed taxa (Table 4). Despite the tendency for instability, parameter error does not translate into wide confidence intervals on seed shadows and densities of α (Fig. 6), due, in part, to correlations.

DISCUSSION

The inverse approach allows us to compete alternative views within a closed canopy, where we cannot directly observe dispersal (Fig. 2). The method allows ''direct'' comparisons. Rather than selecting models based on how much better each does in comparison with a null model known to be wrong, our likelihoods for each model permit direct comparison.

Model competition arbitrated by three data sets suggests a kernel that accommodates a range (mixture) of processes that result in convexity near the source and a fat tail (Figs. 1b, 5). When given the choice between models that assume the ''right'' shape at local scales vs. long distances, the data choose the model that gets both (2Dt) for 14 of 26 species (Table 3). Competing models did better than the 2Dt in cases in which no model provided confident fits (*Tsuga*, *Pinus ponderosa*, and *Spondias mombin* in Table 4). The exceptions,

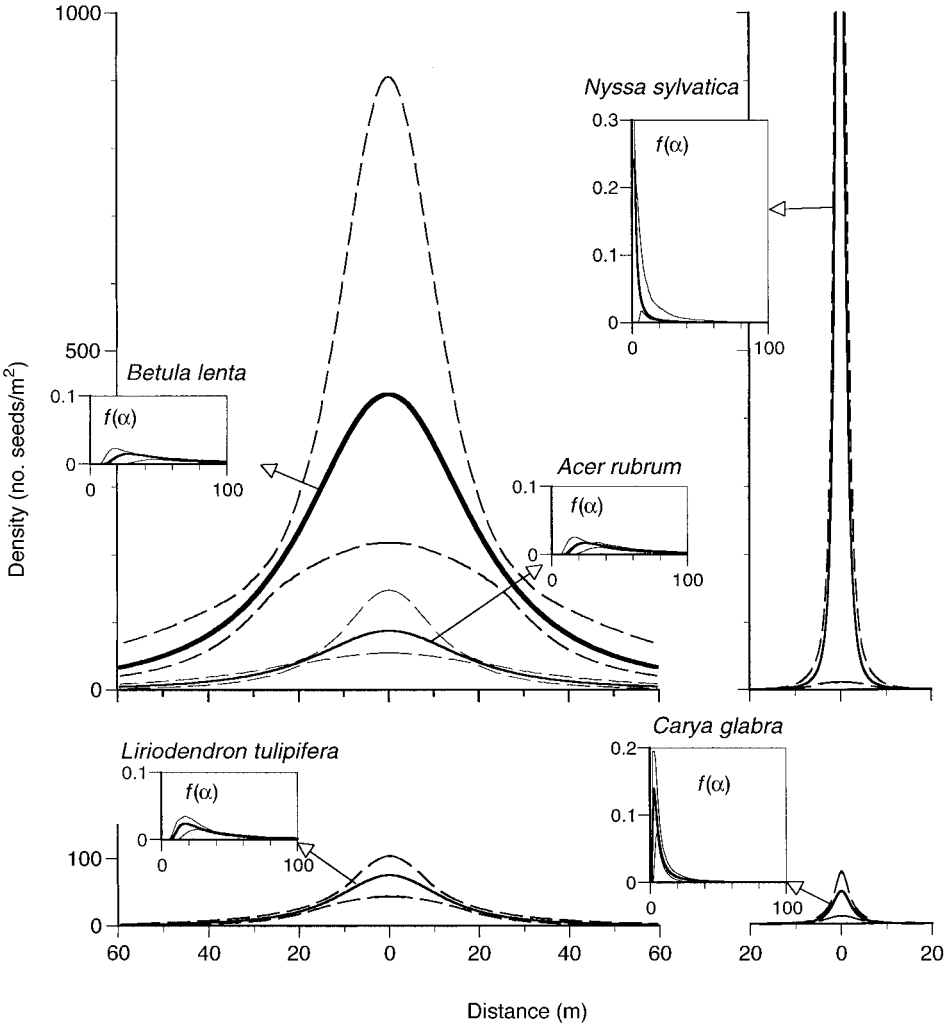

FIG. 6. Example of seed shadows and α densities (insets) with bootstrapped 95% confidence intervals. Animal-dispersed species (right side) contrast with wind-dispersed species (left side) in having seed densities (and α parameter values) clustered near sources.

where fits were best for the Gaussian or a more platykurtic distribution (parameter $c > 2$ in Eq. 3), occurred mostly where seed densities were low (animal-dispersed types) and data were of limited extent (two or four years for temperate mixed-conifer and tropical floodplain).

The tail is hard to estimate (Portnoy and Willson 1993, Clark et al. 1998*b*, Turchin 1998). Extrapolating a tail beyond the data is speculative; to do so from our results would be inappropriate. Plots range from 60 to 150 m on a side, so our data include seeds traveling well beyond direct crown influence. Although the fit is most influenced by the high densities near the source, the 2Dt model has the flexibility to fit these local densities, while simultaneously responding to low densities at distance. Inflexible models (e.g., Gaussian) have a tail shape that is controlled by the preponderance of seed at short distances. Our model comparisons indicate that a flexible kernel can be sensitive to tail shape, and that a fat tail fits the data better than does the alternative.

Data likewise preferred convexity at the source over the concave exponential model. Although concave seed shadows (exponential and power functions) are widely used, we found only one case in which an exponential model provided the best fit (Table 3). Concave models are reasonable at distances beyond the immediate influence of the crown, but they performed worse than the 2Dt model over the scales included here.

In summary, the 2Dt provides a better description of data than do previous models. This flexibility is obtained with few parameters. Our results suggest that, in most cases, the parameter p might be fixed at a low value (e.g., 1 or 1/2), because it lends stability to the likelihood (Eq. 12). With p fixed and only two fitted parameters, the 2Dt kernel is no more complex than

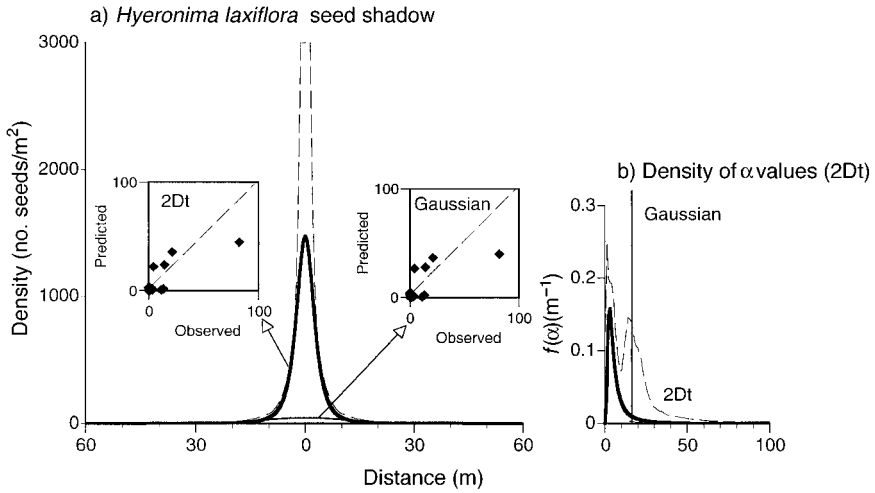

FIG. 7. A fit demonstrating the tendency for model instability when data are sparse; a single seed trap accumulated large densities (insets). Confidence intervals near the source range over several orders of magnitude due to negative parameter correlation (a), and there is tendency for bimodality in the α parameter (b).

Gaussian or exponential models. This advantage of simplicity is no reason to avoid more complex models. Indeed, if and when large data sets come available, it would be valuable to test mechanistic models with more parameters. Because minimal models are a goal of community and global ecology, however, simplicity has advantages.

Dispersal in temperate vs. tropical forests

Our three data sets form continua in diversity and in the importances of animal dispersal and lianas. Our mixed-conifer forest, with low diversity, few lianas, and a preponderance of wind dispersal, contrasts with the tropical floodplain, where diversity is high, lianas are abundant, and dispersal is mostly by vertebrates. The southern Appalachian forest is intermediate in both respects.

Differences among biomes in tree diversity are reflected in seed diversity (Fig. 8a). High diversity in the tropics means that any given species is rare. Mapped plots contain fewer individuals of a species, so seed traps represent less of the variability than they do in our temperate forests. Most tree taxa are represented by only one or two individuals per hectare, and most seed taxa are present in a single trap. Frequency of seed vs. rank abundance shows strong differences among biomes (Fig. 8).

Diversity affects the sampling effort needed to estimate dispersal. In the tropics, dispersal could not be estimated for most taxa, because they were represented by one seed. Seed richness (number of species per plot), including unknown morphotypes, was 284 species on this 2.25 ha plot. Of 72 tree species having at least one individual >10 cm dbh, we obtained dispersal estimates for seven species. By contrast, we obtained dispersal estimates for most species in mixed-conifer and southern Appalachians forests. We obtained few dispersal estimates for any taxa having frequencies of <10 traps (Fig. 8b–d).

Dispersal modes affect estimation. Seed traps are most conducive to estimating wind (passive) dispersal. Primary and secondary dispersal by vertebrates is sporadic, clumped, and, thus, unpredictable. Especially in the tropics, animals (e.g., bats) consume fruits at roosts that can be distant from the parent tree. Secondary dispersal by scatterhoarding mammals is not described by seed traps. The effect of vertebrate dispersal is evident in Fig. 8b, where most seed taxa at frequencies of <20 seed traps are animal dispersed, and the majority originate from outside the 2.25-ha plot. Seeds from species that do not grow on the plot are rare for the other two data sets (Fig. 8c, d). The many lianas in our tropical site are difficult to estimate, because the seeds do not originate from a coherent canopy.

Learning from experience: Bayesian analysis

Dispersal characterization for many species will be limited, for the near future, by data availability. Seed rain is sporadic. Our best fits come from the study area having six years of data from 100 seed traps (temperate deciduous, Table 4). Such data sets are few. Fits for our two other sites would improve with greater duration of sampling, because interannual variability is high (Ruth and Berntsen 1955, Curtis and Foiles 1961, Clark et al., 1999). Correlations between dispersal and seed fall velocity, and between dispersal and fecundity (Clark et al. 1998*b*; Fig. 4 in this study) provide insights that can be broadly applied. Each new analysis might build on previous results toward development of general models.

Bayesian analysis can be used to develop dispersal kernels, demonstrated here with an example. The re-

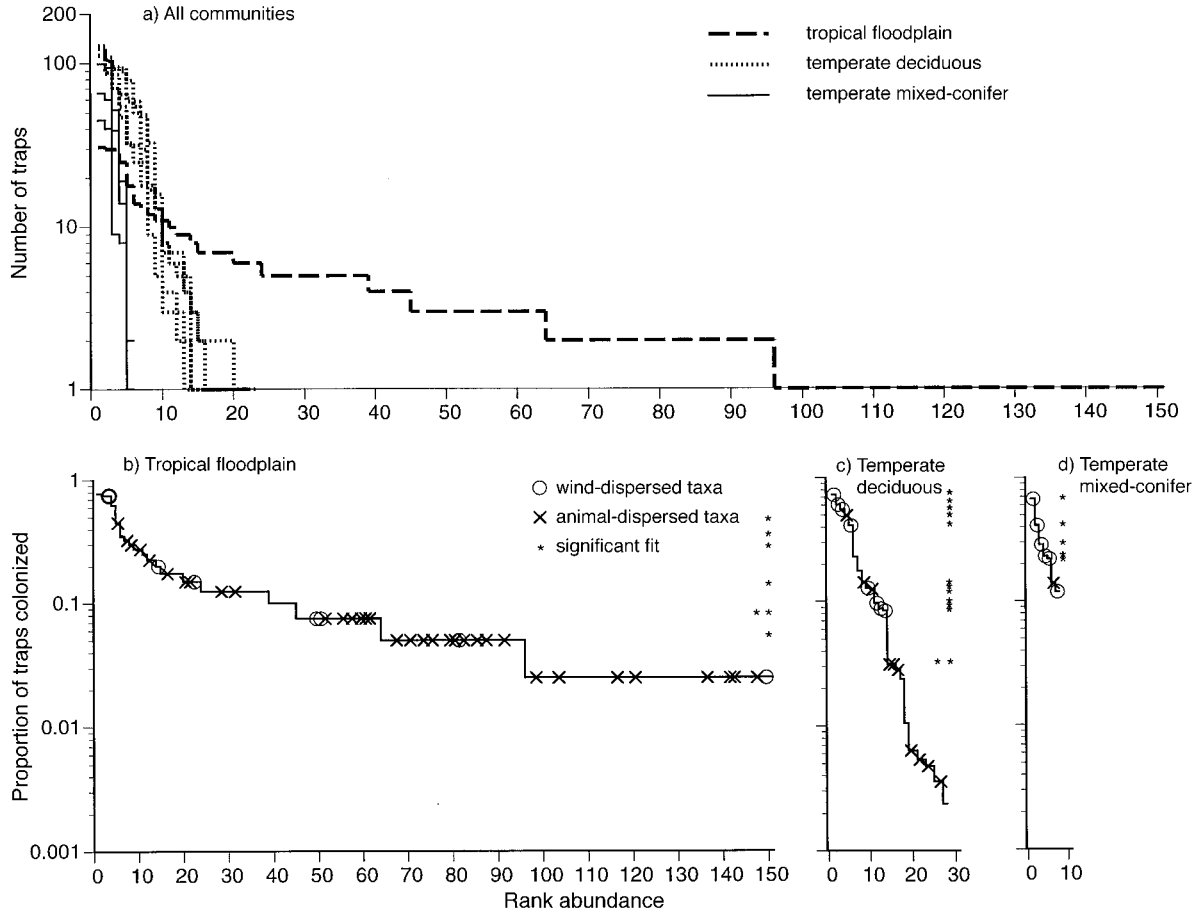

FIG. 8. Frequency of seeds in seed traps plotted against rank abundance for the three data sets. Panel (a) shows all stands and all sites. Panels (b–d) show rank abundances with dispersal vectors, showing seed types for which no trees occurred on the plots, and types having significant fits to one or more dispersal models (indicated by asterisks). For the tropical floodplain (b), most rare taxa come from outside the plot. The temperate forest (c) supports a mixture of animal- and wind-dispersed types. The mixed-conifer forest (d) includes almost exclusively wind-dispersed types. Note the *y*-axis log scale.

lationship between fall velocities and α estimates (Greene and Johnson 1989, Okubo and Levin 1989, Andersen 1991, Clark et al. 1998*b*) suggests that seed type provides initial information on the dispersal parameter. Therefore, we might exploit confident fits for *Pinus rigida* that result from six years of data in the southern Appalachians as a prior for estimating *P. lambertiana* and *P. ponderosa.* One could argue that this prior is biased, because *P. rigida* seeds are smaller (an upward bias in α), or are released from lower heights (a downward bias in α) than are *P. lambertiana* and *P. ponderosa* seeds. We do not defend this particular choice for the prior, as our concern here is simply to demonstrate the approach. (Gelman et al. [1995] review methods for checking the fit with data sets simulated from the posterior density.) The normalized likelihood

$$NL = \frac{L(\mathbf{S}\,|\,\alpha)}{\int_0^\infty f(\alpha)L(\mathbf{S}\,|\,\alpha)\,d\alpha}$$

where **S** is the new data set, and $f(\alpha)$ is a prior density of α (here, based on *P. rigida*), is rather broad for *P. lambertiana* (Fig. 9a) and quite broad for *P. ponderosa* (Fig. 9b). The breadths of these likelihoods do not reflect impossibly great dispersal. Rather, the noise in the data tends to result in relatively flat likelihood surfaces. *P. ponderosa* densities in clearcuts suggest dispersal more restricted than that in Fig. 9b (Barrett 1966). By contrast, the density for *P. rigida* (used here as the prior) is concentrated at short distances. The posterior densities obtained from this Bayesian approach,

$$f(\alpha\,|\,\mathbf{S}) = f(\alpha) \times NL$$

probably represent more realistic descriptions for *P. lambertiana* and *P. ponderosa.* For example, 95% of the density for *P. lambertiana* decreases from (6.1, 76.9) (normalized likelihood) to (4.6, 31.4) (posterior density of α).

Moreover, the functional forms used here are especially attractive for fitting the exponential family. For

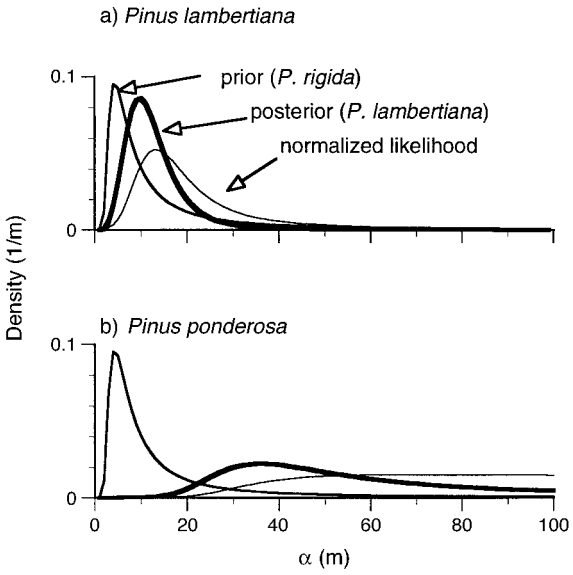

FIG. 9. Bayesian analysis of dispersal parameters using estimates from *Pinus rigida* as a prior for *P. lambertiana* and *P. ponderosa.*

direct estimation (i.e., seed release data), the density for α that derives from our assumptions (Eq. 9) is a conjugate prior for the exponential family of kernels (Eq. 4), thus providing an analytically tractable estimation procedure (Appendix B).

Implications of the 2Dt kernel for recruitment limitation

Theory and models suggest that diversity in plant communities depends on the fraction of seed dispersed beyond the influence of the parent plant (Janzen 1970, Shmida and Ellner 1984, Clark and Ji 1995, Pacala et al. 1997). The role of dispersal in many such models can be traced to how it affects the balance between intra- and interspecific competition. Seed remaining close to the adult increases intraspecific competition, both directly (inhibition by the parent and sib competition) and indirectly (frequency- or density-dependent predation and pathogens). Distant dispersal contributes more to interspecific competition. Coexistence is promoted when restricted dispersal limits interspecific competition below that which prevails in a ''well-mixed'' community.

Although fitted to the same data sets, the 2Dt model predicts a different balance between local and nonlocal dispersal than do the Gaussian (Clark et al. 1998*a*) or more platykurtic (Ribbens et al. 1994) kernels (Fig. 9). The fraction of seed dispersed beyond radius R is given by $\int_R^\infty \oint_{2\pi} f(r, \theta)\, d\theta\, dr$. For the 2Dt kernel, that fraction is

$$\left(\frac{u}{u + R^2}\right)^p.$$

In the limit as p becomes large, this tends to the Gaussian result:

$$\exp\left[-\left(\frac{R}{\alpha}\right)^2\right].$$

Fig. 10 demonstrates substantial differences between the predictions of these two models for our parameters. For the same data sets, the Gaussian kernel substantially overestimates the fraction dispersed beyond the influence of 5 m radius crowns. The bias is severe for poorly dispersed types and negligible for well-dispersed types (Fig. 10b). The Gaussian kernel underestimates the fraction dispersed outside the patch sizes typically employed in gap models (Fig. 10c). Depending on the spatial scale, inaccurate kernel shapes will bias the balance between intra- and interspecific competition.

Implications for population spread

The shape of the tail controls population spread. A shift in migration potential from diffusion to accelerating spread occurs as the tail fattens beyond the exponential bound (Fig. 1; see Mollison 1972, Kot et al. 1996). The Gaussian model approaches zero rapidly with distance, making migration a coherent, stepwise process, paced by the dispersal parameter α and the rate of population increase. This coherent spread breaks down for fat-tailed dispersal kernels, producing a noisy, irregular, and accelerating spread (Lewis 1997, Clark et al. 1998*a*). Clark et al. (1998*a*) suggested that fat-tailed dispersal kernels might explain the high rates of spread of tree populations at the end of the Pleistocene ($>10^3$ m/yr), an explanation consistent with speculations of previous authors (Davis 1987). Such rates are consistent with observed dispersal (Clark 1998). Our finding here that fat-tailed kernels actually provide the best description of dispersal in forest stands bolsters the interpretation that population spread could be rapid in response to climate changes in the past and future. The shapes of these kernels suggest that predicting responses to future climate change (e.g., Leishman et al. 1992, Pitelka et al. 1997, Clark et al. 1998*a*) will depend on understanding the processes that govern the tail of the dispersal kernels, i.e., the tails of the α distributions in Fig. 6.

CONCLUSIONS

Finding a kernel that predicts more realistic patterns and that fits the data better than do classical models does not mean that we have fully acquired the tools needed for analysis of dispersal at all scales. Our results describe dispersal at local and ''intermediate'' spatial scales. We state parameter confidence, and we translate that degree of confidence to the seed shadows themselves. That description helps us to interpret how seed shadows influence community dynamics (Fig. 8), including recruitment limitation (Ribbens et al. 1994, Clark et al. 1998*b*), and the qualitative patterns of pop-

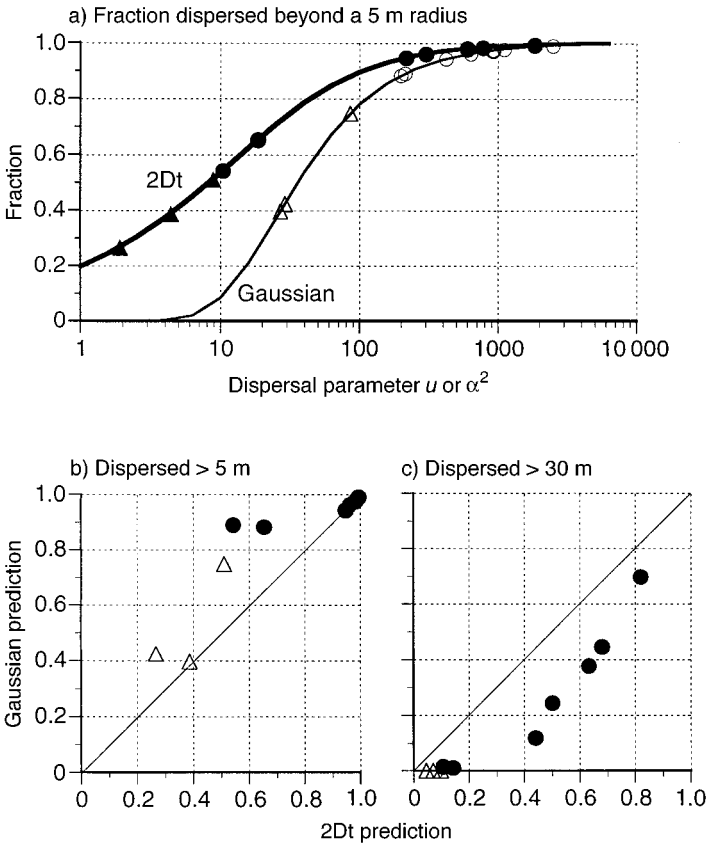

FIG. 10. Predicted fraction of seed dispersed beyond radii of 5 m (a, b) and 30 m (c) for Gaussian and 2Dt models with parameter $p = 0.5$. (a) Both models predict an increasing fraction of seed beyond the 5-m radius with increasing dispersal parameter (u or α). Symbols represent actual fits for the two models. Solid symbols are the 2Dt model. Triangles represent animal-dispersed seed, and circles represent wind-dispersed seed. The Gaussian model overpredicts the fraction of seed traveling beyond 5 m (b) but underestimates the fraction traveling beyond 30 m (c).

ulation spread that might be expected with climate change (Clark et al. 1998*a*). Our results do not fully resolve the need for dispersal data at regional scales, because we cannot safely extrapolate a kernel parameterized at the 10^2-m scale to whole regions. For many problems, however, including population spread, such extrapolation is not as critical at it might first appear. Clark (1998) found that the fat-tail kernels can cause accelerating spread to rates exceeding 10^2 m/yr, even when the kernel is truncated at 10^3 m. Although this distance exceeds the sizes of mapped plots used to parameterize our kernels, it demonstrates that ''infinite tails'' are not required for rapid spread. Seed dispersal up to 10 km is plausible for many species during severe storms and when transported by frugivorous birds and bats, corvids that cache fagaceous nuts, and large vertebrates, such as bears, elephants, rhinos, foxes, and primates.

Just as important as the specific results relating to a new model is the methodology for competing alternative models, as new data sets and mechanistic interpretations become available. Our inverse approach is not bound to the particular models that we analyzed here, or to a particular scale. Spatial relationships between offspring and parents can be used to translate the composite pattern of seed rain to the forest floor into seed shadows for individual plants (Fig. 2) and distributions of dispersal parameters (Fig. 7). Such relationships can be parameterized at much broader scales than attempted here, including ones of relevance for analysis of migration and forest recovery from fragmentation.

ACKNOWLEDGMENTS

Field sampling and lab analysis were assisted by Brenda Cleveland and the research staff of the USGS Sequoia and Kings Canyon Field station. John Terbourg provided the stem map data for the Tropical floodplain site. For helpful discussion and/or comments on the manuscript, we thank Brian Beckage, Brenda Cleveland, Philip Dixon, Mark Lewis, Chris Paciorek, Pete Wyckoff, and two anonymous reviewers. The research was supported by NSF grants BSR-9444146, DEB 9453498, and DEB-9632854 to J. S. Clark and by a DOE Global Change Graduate Fellowship administered by the Oak Ridge Institute for Science and Education to R. Kern.

LITERATURE CITED

Andersen, M. 1991. Mechanistic models for the seed shadows of wind-dispersed plants. American Naturalist **137**: 476–497.

Augspurger, C. K., and S. E. Franson. 1987. Wind dispersal of artificial fruits varying in mass, area, and morphology. Ecology **68**:27–42.

Augspurger, C. K., and S. E. Franson. 1988. Input of wind-dispersed seeds into light gaps and forest sites in a Neotropical forest. Journal of Tropical Ecology **4**:239–252.

Augspurger, C. K., and K. Kitajima. 1992. Experimental studies of seedling recruitment from contrasting seed distributions. Ecology **73**:1270–1284.

Balanda, K. P., and H. L. MacGillivray. 1988. Kurtosis: a critical review. American Statistician **42**:111–119.
Barrett, J. W. 1966. A record of ponderosa pine seed flight. U.S. Forest Service Pacific Northwest Forest and Range Experiment Station **PNW-38**:1–5.
Bjorkbom, J. C. 1971. Production and germination of paper birch seed and its dispersal into a forest opening. U.S. Forest Service Research Paper **NE-209**:1–14.
Carkin, R. E., J. F. Franklin, J. Booth, and C. E. Smith. 1978. Seeding habits of upperslope tree species. IV. Seed flight of noble fir and Pacific silver fir. U.S. Forest Service Pacific Northwest Forest and Range Experiment Station Research Note **PNW-312**:1–10.
Chernoff, H. 1954. On the distribution of the likelihood ratio. Annals of Mathematical Statistics **25**:573–578.
Clark, J. S. 1998. Why trees migrate so fast: confronting theory with dispersal biology and the paleo record. American Naturalist **152**:204–224.
Clark, J. S., B. Beckage, P. Camill, B. Cleveland, J. HilleRisLambers, J. Lichter, J. MacLachlan, J. Mohan, and P. Wyckoff. 1999. Interpreting recruitment limitation in forests. American Journal of Botany **86**:1–16.
Clark, J. S., C. Fastie, G. Hurtt, S. T. Jackson, C. Johnson, G. King, M. Lewis, J. Lynch, S. Pacala, I. C. Prentice, E. W. Schupp, T. Webb III, and P. Wyckoff. 1998*a*. Reid's Paradox of rapid plant migration. BioScience **48**:13–24.
Clark, J. S., and Y. Ji. 1995. Fecundity and dispersal in plant populations: implications for structure and diversity. American Naturalist **146**:72–111.
Clark, J. S., E. Macklin, and L. Wood. 1998*b*. Stages and spatial scales of recruitment limitation in southern Appalachian forests. Ecological Monographs **68**:213–235.
Curtis, J. D., and M. W. Foiles. 1961. Ponderosa pine seed dissemination into group clearcuttings. Journal of Forestry **59**:766–767.
Davis, M. B. 1981. Quaternary history and the stability of forest communities. Pages 132–153 *in* D. C. West, H. H. Shugart, and D. B. Botkin, editors. Forest succession: concepts and application. Springer-Verlag, New York, New York, USA.
———. 1987. Invasion of forest communities during the Holocene: beech and hemlock in the Great Lakes region. Pages 373–393 *in* A. J. Gray, M. J. Crawley, and P. J. Edwards, editors. Colonization, succession, and stability. Blackwell Scientific, Oxford, UK.
Efron, B., and R. J. Tibshirani. 1993. An introduction to the bootstrap. Chapman and Hall, New York, New York, USA.
Fastie, C. L. 1995. Causes and ecosystem consequences of multiple pathways of primary succession at Glacier Bay, Alaska. Ecology **76**:1899–1916.
Fowells, H. A., and G. H. Schubert. 1956. Seed crops of forest trees in the pine region of California. USDA Technical Bulletin **1150**:1–48.
Gelman, A., J. B. Carlin, H. S. Stern, and D. B. Rubin. 1995. Bayesian data analysis. Chapman and Hall, London, UK.
Geritz, S. A. H., T. J. de Jong, and P. G. L. Klinkhamer. 1984. The efficacy of dispersal in relation to safe site area and seed production. Oecologia **62**:219–221.
Gladstone, D. E. 1979. Description of a seed-shadow of a wind-dispersed tropical tree. Brenesia **16**:81–86.
Green, D. S. 1983. The efficacy of dispersal in relation to safe site density. Oecologia **56**:356–358.
Greene, D. F., and E. A. Johnson. 1989. A model of wind dispersal of winged or plumed seeds. Ecology **70**:339–347.
Guevara, S., and J. Laborde. 1993. Monitoring seed dispersal at isolated standing trees in tropical pastures: consequences for local species availability. Vegetatio **107/108**:319–338.
Holthuijzen, A. M. A., and T. L. Sharik. 1985. The red cedar (*Juniperus virginiana* L.) seed shadow along a fenceline. American Midland Naturalist **113**:200–202.
Houle, G. 1992. Spatial relationship betweeen seed and seedling abundance and mortality in a deciduous forest of north-eastern North America. Journal of Ecology **80**:99–108.
Hughes, J. W., and T. J. Fahey. 1988. Seed dispersal and colonization in a disturbed northern hardwood forest. Bulletin of the Torrey Botanical Club **115**:89–99.
Hurtt, G. C., and S. W. Pacala. 1995. The consequences of recruitment limitation: reconciling chance, history and competitive differences between plants. Journal of Theoretical Biology **176**:1–12.
Janzen, D. H. 1970. Herbivores and the number of tree species in tropical forests. American Naturalist **104**:501–528.
Johnson, W. C. 1988. Estimating dispersibility of *Acer, Fraxinus,* and *Tilia* in fragmented landscapes from patterns of seedling establishment. Landscape Ecology **1**:175–187.
Kot, M., M. A. Lewis, and P. van den Driessche. 1996. Dispersal data and the spread of invading organisms. Ecology **77**:2027–2042.
Lamont, B. 1985. Dispersal of the winged fruits of *Nuytsia floribunda* (Loranthaceae). Australian Journal of Ecology **10**:187–193.
Leishman, M., L. Hughes, K. French, D. Armstrong, and M. Westoby. 1992. Seed and seedling biology in relation to modelling vegetation dynamics under global climate change. Australian Journal of Botany **40**:599–613.
Levin, S. A. 1976. Population dynamics in heterogeneous environments. Annual Review of Ecology and Systematics **7**:287–310.
Levin, S. A., D. Cohen, and A. Hastings. 1984. Dispersal in patchy environments. Theoretical Population Biology **26**: 165–191.
Lewis, M. A. 1997. Variability, patchiness and jump dispersal in the spread of an invading population. Pages 46–69 *in* D. Tilman and P. Kareiva, editors. Spatial ecology. Princeton University Press, Princeton, New Jersey, USA.
Mair, A. R. 1973. Dissemination of tree seed: Sitka spruce, western hemlock, and Douglas-fir. Scottish Forestry **27**: 308–314.
Mardia, K. V. 1970. Measures of multivariate skewness and kurtosis with application. Biometrika **57**:519–530.
Martinez-Ramos, M., and A. Soto-Castro. 1993. Seed rain and advanced regeneration in a tropical rain forest. Vegetatio **107/108**:299–318.
Matlack, G. R. 1987. Diaspore size, shape, and fall behavior in wind-dispersed plant species. American Journal of Botany **74**:1150–1160.
Mollison, D. 1972. The rate of spatial propagation of simple epidemics. Proceedings of the Sixth Berkeley Symposium on Mathematics, Statistics, and Probability **3**:579–614.
———. 1977. Spatial contact models for ecological and epidemic spread. Journal of the Royal Statistical Society Series B **39**:283–326.
Mosteller, F., and J. W. Tukey. 1977. Data analysis and regression. Addison-Wesley, Reading, Massachusetts, USA.
Okubo, A., and S. A. Levin. 1989. A theoretical framework for data analysis of wind dispersal of seeds and pollen. Ecology **70**:329–338.
Pitelka, L. F., et al. 1997. Plant migration and climate change. American Scientist **85**:464–473.
Portnoy, S., and M. F. Willson. 1993. Seed dispersal curves: behavior of the tail of the distribution. Evolutionary Biology **7**:25–44.
Ribbens, E., J. A. Silander, and S. W. Pacala. 1994. Seedling recruitment in forests: calibrating models to predict patterns of tree seedling dispersion. Ecology **75**:1794–1806.
Ritchie, J. C., and G. M. MacDonald. 1986. The patterns of post-glacial spread of white spruce. Journal of Biogeography **13**:527–540.
Ruth, R. H., and C. M. Berntsen. 1955. A 4-year record of Sitka spruce and western hemlock seed fall on the Cascade

Head Experimental Forest. U.S. Forest Service Pacific Northwest Forest and Range Experiment Station Research Paper **12**:1–13.
Schupp, E. W. 1990. Annual variation in seedfall, postdispersal predation, and recruitment of a neotropical tree. Ecology **71**:504–515.
Sharpe, D. M., and D. E. Fields. 1982. Integrating the effects of climate and seed fall velocities on seed dispersal by wind: a model and application. Ecological Modelling **17**: 297–310.
Shmida, A., and S. Ellner. 1984. Coexistence of plant species with similar niches. Vegetatio **58**:29–55.
Stuart, A., and J. K. Ord. 1994. Kendall's advanced theory of statistics. Edward Arnold, New York, New York, USA.
Turchin, P. 1998. Quantitative analysis of movement. Sinauer, Sunderland, Massachusetts, USA.
Venable, D. L., and J. S. Brown. 1993. The population-dynamic functions of seed dispersal. Vegetatio **107/108**: 31–55.
Willson, M. F. 1993. Dispersal mode, seed shadows, and colonization patterns. Vegetatio **107/108**:261–280.

APPENDIX A

Moments and Indices Derived from Them

To compare dispersal kernels, we require an index that quantifies shape. Although the term ''kurtosis'' evokes this notion of shape, there is no standard index that enjoys general acceptance. In this Appendix, we summarize the concept and propose a simple measure for the case at hand, i.e., a bivariate dispersal kernel with rotational symmetry.

Kurtosis ''can be vaguely defined as the location and scale-free movement of probability mass from the shoulders of a distribution to its center and tails'' (Balanda and MacGillivray 1988: 111), and can be formalized in many ways (see also Mosteller and Tukey 1977). One class of measures is based on moments. Moments are expected values of powers of a variable, which, in some sense, summarize distribution shape. The mean, variance, skewness, and kurtosis involve the first through fourth moments, respectively. The fourth central moment standardized for variance is the most common kurtosis measure for univariate distributions, but it has an unclear relationship to shape, and a given value can correspond to more than one distribution. Moreover, the method used to quantify a shift of mass from the shoulders to peak and tails (scaling) affects the value. (The squared variance is the scaling option often used for moment-based measures.) The problems are more complex for bivariate distributions, which involve product moments. Despite absence of convention, there is general agreement that kurtosis measures should be independent of scale and location. Beyond these criteria, the index needs to convey useful information regarding shape.

Here, we describe our moment-based index that is simple and appropriate for this application (bivariate, rotationally symmetric distributions in polar coordinates), that is scale and location-invariant, and that allows comparisons with standard distributions (e.g., Gaussian, exponential). Our moment-based method begins with one for bivariate distributions (Mardia 1970) included in a standard reference (Stuart and Ord 1994), but follows with an argument for simplification. We solve for Mardia's bivariate moments and then demonstrate that the useful information for symmetric distributions is fully summarized by the simpler (marginal) moments about distance r.

Shape measures for bivariate kernels

Mardia (1970) suggests a measure of kurtosis for the bivariate case:

$$k = \frac{\mu_{40}}{\mu_{20}^2} + \frac{\mu_{04}}{\mu_{02}^2} + \frac{2\mu_{22}}{\mu_{20}\mu_{02}}, \quad \text{(A.1)}$$

where $\mu_{m,n}$ is mth and nth central moment over two random variables. This formula is typically applied (see examples in Mardia 1970 and Stuart and Ord 1994) to distributions defined on the Cartesian plane for random variables (x, y). For the 2Dt case, we substitute $r^2 = x^2 + y^2$ in Eq. 8 and take moment integrals to obtain the following complex expression:

$$\mu_{rs} = \frac{u^p p}{\pi} \int_{-\infty}^{\infty}\int_{-\infty}^{\infty} \frac{x^m y^n \, dy \, dx}{[u + x^2 + y^2]^{p+1}}$$
$$= \frac{u^{(m+n)/2}\Gamma\left(\frac{m+1}{2}\right)\Gamma\left(\frac{n+1}{2}\right)\Gamma\left(p - \frac{m+n}{2}\right)}{\pi\Gamma(p)}. \quad \text{(A.2)}$$

The resulting kurtosis from the three terms of A.1 is

$$k(x, y) = \frac{3(p-1)}{p-2} + \frac{3(p-1)}{p-2} + \frac{2(p-1)}{p-2}. \quad \text{(A.3)}$$

For instance, a Gaussian dispersal kernal (obtained in the limit $p \to \infty$) yields a value of 8 for the Cartesian coordinates (x, y).

The bivariate moments (Eq. A.2) for the rotationally symmetric kernels that dispersal biologists typically consider are unnecessarily complex and redundant. The complexity of bivariate moments for the Cartesian locations x and y is undesirable, because (1) the variable r (distance from the source) is meaningful, whereas location (x, y) is meaningful only indirectly; and (2) the solution for r is simple, whereas the moments of (x, y) can be complex (e.g., Stuart and Ord 1994). The first of these two claims is borne out by the fact that seed dispersal is usually reported as distance from the source, not as Cartesian coordinates. The three terms in Eq. A.3 come from the marginal distribution of x, from the marginal distribution of y, and from cross products, respectively. Each describes the same influence of shape parameter p, i.e., $(p - 1)/(p - 2)$. We can learn from any one of these terms that kurtosis is finite so long as $p > 2$, and that kurtosis declines to an asymptote as p becomes large. Thus, a measure based on bivariate moments is unnecessarily complex.

Given that bivariate moments add redundancy, but not insight, we consider marginal (univariate) moments of distance r. A simple kurtosis measure for rotationally symmetric distributions is obtained by first integrating the non-informative arc angle out of existence and then solving the moment integral for the marginal density $2\pi f_{2\pi}(r)$:

$$\mu_m = \int_0^{\infty}\oint_{2\pi} r^m f(r, \theta) \, d\theta \, dr = 2\pi \int_0^{\infty} r^{m+1} f_{2\pi}(r) \, dr$$
$$= \frac{2p}{u}\int_0^{\infty} \frac{r^{m+1}}{\left[1 + \frac{r^2}{u}\right]^{p+1}} \, dr. \quad \text{(A.4)}$$

The substitution $v = r^2/u$ yields

$$\mu_m = u^{m/2} p \int_0^{\infty} \frac{v^{m/2}}{(1+v)^{p+1}} \, dv.$$

Recognizing the integral expression as a beta function,

$$B(a, b) = \int_0^\infty \frac{z^{a+1}}{(1 + z)^{a+b}}\, dz = \frac{\Gamma(a)\Gamma(b)}{\Gamma(a + b)}$$

we obtain a simple expression for the mth moment:

$$\mu_m = u^{m/2} pB\left(1 + \frac{m}{2},\ p - \frac{m}{2}\right).$$

Because arguments of the beta function involve integers (moments), it is convenient to recast this result in terms of gamma functions:

$$\mu_m = \frac{mu^{m/2}\Gamma(m/2)\Gamma(p - m/2)}{2\Gamma(p)}. \tag{A.5}$$

Kurtosis is the first term of Eq. A.1:

$$\underset{(2\text{Dt})}{k(r)} = \frac{\mu_4}{\mu_2^2} = \frac{2(p - 1)}{p - 2}. \tag{A.6a}$$

This compares with that for the exponential family:

$$\underset{(\text{exponential family})}{k(r)} = \frac{\Gamma(6/c)\Gamma(2/c)}{\Gamma^2(4/c)}. \tag{A.6b}$$

Both are scale and location-invariate, involving only the dimensionless shape parameters p and c, respectively.

One aspect of our foregoing approach deserves mention. Because r is the distance from the mean of a rotationally symmetric density, Eq. A.4 represents ''central'' moments, in the sense that they are taken about the mean of the dispersal kernel. They are not centered on the mean of r, because those moments would be hard to relate to the density symmetric about $r = 0$. Because moments are centered on zero, rather than the mean of r, odd moments are not zero; r is the distance traveled in any direction (we begin the derivation of Eq. A.3 by integrating arc angle out of existence). Although the numerical values of moments of r (Eq. A.6a) differ from those of (x, y) (Eq. A.3), they summarize the same quantity. For example, the existence of moments of r implies finite moments in Cartesian space (compare Eqs. A.2 and A.5).

The marginal moments of r (Eq. A.5) and the kurtosis measure that is based on them (Eq. A.6) capture the essential features of kernel shape. The simplicity and insight of Eq. A.6 recommends it as a general shape measure for rotationally symmetric dispersal kernels.

Shape comparisons

Eqs. A.6a and A.6b allow comparison of kernel shape for the two densities considered here. For the 2Dt density, moments smaller than $2p$ are finite, and kurtosis tends to infinity as p decreases to 2 (Eq. A1.6a). Kurtosis asymptotes at 2 as p becomes large (the Gaussian limit). Potentially large kurtosis results from the fact that the tail can be extremely fat, precluding convergence of moment integrals. For the exponential family, kurtosis is finite, tending to large values as c tends to zero. Values are 2 and 3.33 for Gaussian ($c = 2$) and exponential ($c = 1$), respectively. Distributions that are more peaked and fatter tailed than exponential have kurtosis measures >3.33. This value is important in migration studies, because it represents the point at which traveling wave solutions yield to accelerating spread (Mollison 1977). Other kernels in the exponential family used to model dispersal include $c = 3$ (Ribbens et al. 1994) and $c = 1/2$ (Kot et al. 1996, Clark 1998), with kurtosis values from Eq. A.6b of 1.70 and 9.43, respectively.

APPENDIX B

A Bayesian Link to Direct Kernel Estimation

The inverse approach is applied to spatial patterns of seed rain having a complex, distributed source. The model developed here can also be applied to the direct approach, in which seeds are released and settling distances r are recorded (e.g., Augspurger and Franson 1987, Matlack 1987). We demonstrate the connection between variability in α and kernel shape, as represented by our densities $f(\alpha)$ and $f(r\,|\,\alpha)$, in a Bayesian context. To simplify our likelihood, we assume that all released seed is recovered. This assumption allows us to write a likelihood based directly on the density of r, as opposed to a binomial (with some probability of recovery) within which $f(r)$ is embedded.

The 2Dt model involves a conjugate prior

Assume that seed is dispersed according to an exponential kernel family. The sampling distribution is given by Eq. 4. Assuming that the variable

$$A = \frac{\nu}{\alpha^c}$$

is gamma distributed, we use the previous approach to obtain the prior density of α:

$$f(\alpha) = \frac{cu_0^p}{\alpha^{cp+1}\Gamma(p)}\exp\left[-\frac{u_0}{\alpha^c}\right], \tag{B.1}$$

where u_0 is our prior estimate of u. Integrating Eq. 4 over variability in α gives the marginal density for this exponential family:

$$f(r) = \int_0^\infty f(\alpha) f(r\,|\,\alpha)\, d\alpha = \frac{cu^p}{2\pi B(2/c, p)(u + r^c)^P}$$

where $P = 2/c + p$.

The likelihood of observing n seeds, each of which travels distance r_i, is given by

$$f(\mathbf{r}\,|\,\alpha) = \prod_{i=1}^{n} f(r_i|\alpha) = \frac{c^n}{2^n\pi^n\alpha^{2n}\Gamma^n(2/c)}\exp\left[-\frac{1}{\alpha^c}\sum_{i=1}^{n} r_i^c\right] \tag{B.2}$$

and the marginal density is

$$f(\mathbf{r}) = \frac{c^n u_0^p \Gamma(P_n)}{2^n\pi^n\Gamma^n(2/c)\Gamma(p)U_n^{P_n}}$$

where $U_n = u_0 + \Sigma_{i=1}^n r_i^c$ and $P_n = 2n/c + p$. The posterior density is also inverse χ^2:

$$f(\alpha\,|\,\mathbf{r}) = \frac{cU_n^{P_n}}{\alpha^{cP_n+1}\Gamma(P_n)}\exp\left[-\frac{U_n}{\alpha^c}\right] \tag{B.3}$$

which has the same form as Eq. B.1, thus showing Eq. B.1 to be a conjugate prior for the exponential family $f(\mathbf{r}\,|\,\alpha)$. The prior estimate of u_0 has a contribution equivalent to $1/n$. It is further evident from Eq. B.3 that the posterior becomes increasingly peaked with increasing sample size, and the kernel $f(r)$ tends to the exponential family.

Example

A simple data set demonstrates application of the direct method. Dispersal distances of *Fraxinus americana* seeds were recorded from the point of release at a height of 4 m on a calm day. Wind speeds during the experiment ranged from 0 to 0.7 m/s and averaged 0.2 m/s. Seeds were released three times in groups of five to produce the vector of radii

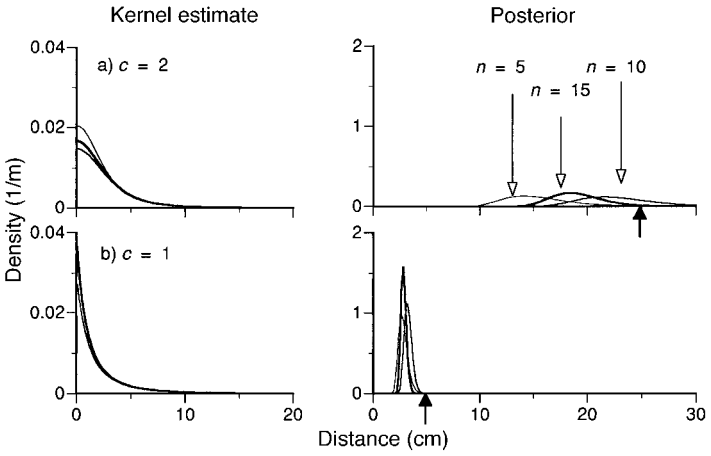

FIG. B1. Dispersal kernel $f(r)$ and Bayesian posterior $f(\alpha \mid \mathbf{r})$ estimates after sequential addition of 5, 10, and 15 observations from data in the *Example*. Prior estimates are indicated by black arrows for these Gaussian (top panel, a) and exponential (bottom panel, b) kernels.

r = (22, 27, 35, 53, 54, 64, 67, 36, 88, 92, 8, 10, 12, 15, 33).

Two examples are shown for parameter values of $c = 2$ (Fig. B1a) and $c = 1$ (Fig. B1b), updated after collection of each of three data sets. Prior estimates of $u_0 = 5^c$ were used for these examples, although results are insensitive to it. As data are added, posterior densities become increasingly peaked, and dispersal kernels estimated from the posterior mean show modest adjustment. Continuing to add data in this manner rapidly leads to focused posterior density with tight confidence intervals.